Investigation on the relationship between NbC and wear-resistance of Fe matrix composite coatings with different C contents

Zhao Changchun [a], Zhou Yefei [a,b], Xing Xiaolei [a], Liu Sha [a], Ren Xuejun [c], Yang Qingxiang [a,]

ABSTRACT

The wear resistance of Fe-based composite coating is significantly related with the character of carbides and matrix, which could be strongly affected by C content in it. In this work, the Fe-based composite coatings with different C contents were prepared. The micro-structure and phase structure of the coatings were analyzed by scanning electron microscope (SEM) equipped with an energy-dispersive spectroscopy (EDS) and X-ray diffractometer (XRD). The hardness and wear resistance of the coatings were determined. Then the hardness and brittleness of carbon poor niobium carbides were calculated by first principles calculation. The results show that, the phase structures of the coatings are mainly composed of NbC, c phase (retained austenite) and a phase (martensite). With the increase of C content, the retained austenite appears and C content of martensite is increased. The hardness of the coatings are increased from HRC 22 to HRC 59. The distribution and morphology of NbC are changed with the increase of C con-tent. The NbC precipitated in reticular grain boundary can be observed when C content is 0.4 wt.% C (C-1). NbC turn into granular and small rod morphology when C content increases to 0.8 wt.% C (C-2). The cracks and defects cannot been found on the surface of the coating when C content is 1.2 wt.% C(C-3), whose hardness is HRC 58 and wear loss is 0.27 g/N cm2 in 8 h. The flaky M7C3 carbide precipitates on the coating when C content is 1.4 wt.% C(C-4), which weaken the wear resistance of the matrix. Compared with the hard-facing coatings with different C contents, the C-3 coating processes higher hardness and wear resistance.

1,Introduction

For its excellent characteristics, such as high hardness, excellent wear resistance and outstanding corrosion resistance, metal matrix composite (MMC) coating is widely applied in surface modification of metal materials. Generally, carbide, nitride, boride and oxide, etc [1–3] were added into the matrix of iron, aluminum, titanium, nickel, etc [2,4,5] as reinforcing phases to prepare composite coatings. Compared to all the matrix material, Fe-based composites coatings has a significant advantage of price. Niobium carbide (NbC) is commonly used as a reinforcement material because of its high hardness, excellent wear resistance [6–8]. Moreover, NbC equip with a similar density compared with iron matrix of coatings, which could promote the distribution uniformity of NbC in coatings [9]. Hence, a number of researchers were attracted to investigate the NbC reinforced iron matrix coatings [10–16]. Hard-facing prepared by GMAW (gas metal arc welding) technology has the advantages of high quality, high efficiency, good adhesion and low price [17]. It could be used to repair failure parts and strengthen the surface of the special parts, which can promote the establishment of a resource-saving, environment-friendly manufacture.

The properties of composite materials are greatly related with the performance of NbC and matrix. As known, the hardness and substructure of martensite in steel can be affected by C content strongly. The change of the character and morphology of iron caused by C content has been investigated by researchers [18,19]. A chain of lath martensite, plate martensite, acicular martensite, lenticular martensite have been observed with C content range 0C–1.8C [20–23]. Jang [24] researched the stability of (Ti,M)C and M(C,Va) carbides (Va equal to C vacancy) by first principle calculation and indicate that carbon vacancies can decrease the lattice parameter and stability of Nb(C,Va) carbides. It is seems that C content was an important factor for the micro-structure and properties change of both iron matrix and carbides.

First-principles calculation based on density functional theory (DFT) is an effective method for structure and mechanical proper-ties study. Xu [25] studied the effects Ti substitutional additions on the mechanical properties of b-Ta5Si3 by theoretical calculation and found that the (Ta0.902Ti0.098)5Si3 could achieve the optimum mechanical properties. Zhang [26] investigated mechanical proper-ties of Fe7-xCrxC carbide and indicated that Fe4Cr3C carbide has a ductile property and has higher hardness than other carbides. Mediukh [27] researched the mechanical properties of Ti-Nb-B2 solid solutions and found that the calculation results of Bulk modulus, Young's modulus, B/G ratio, Vickers hardness and ideal shear strength were decrease from TiB2 to NbB2.

In this work, NbC reinforced Fe-based composite coatings with different C contents were investigated by experiments and first-principles calculation. The relationship between NbC and wear resistance of Fe-based composite coatings was discussed in details.

2. Experimental methods and computational details

2.1Experimental methods

Four Fe matrix composite coatings with different C contents were prepared by welding deposition hard-facing technology [28]. The compositions of the coatings are listed in Table 1.

The micro-structure characterization and worn surfaces morphology of coatings were performed with a HITACHI S4800 field emission scanning electron microscope (FESEM) equipped with EMAX energy dispersive spectrometer (EDS). The phase identification of the coatings was carried out on a Rigaku D/Max-2500/PC X-ray diffraction (XRD) with CuKa operating at 40 KV. The micro-hardness was measured on the cross section of the coating with a load of 200 g for 10 s by FM-ARS 9000 micro-hardness tester. Wear resistance test was evaluated by abrasive belt type wear testing machine in dry friction and SiC of 40 mesh was used as the abrasive material. The wear velocity, loading fore and specimen size are 1.8 104 mm/min, 100 g and 20 mm 10 mm 15 mm, respectively. Micro-hardness was obtained by the averages of ten measurements and wear loss values were obtained by the averages of six measurements.

2.2. Computational details

First-principles calculations based on density functional theory (DFT) with ultrasoft pseudopotentials were employed to evaluate some mechanical properties of carbon poor niobium carbide by using Cambridge Sequential Total Energy Package (CASTEP) [29]. Generalized gradient approximation (GGA) with the Perdew-Burke-Ernzerhof (PBE) functional was employed as exchange-correlation function [30]. On the basis of convergence tests, a plane-wave cutoff energy 350 eV was selected and Brillouin zone sampling was set at 16 16 16 Monkhorst-Pack mesh. The mechanical parameters, bulk modulus and shear modulus were calculated by the Voigt-Reuss-Hill (VRH) approximation method [31].

The equilibrium phase diagram of the system was calculated by Thermo-Calc software (databases: TCFE7). The calculation elements contents were based on C-1 coating.

Coatings compositions (wt.%).

Coatings	C	Cr	Nb	Mn	Si	V	Ti	Fe
C-1	0.4	5.4	4.5	1.1	1.2	0.6	0.3	Bal.
C-2	0.8	5.3	4.4	1.2	1.5	0.5	0.3	Bal.
C-3	1.2	5.4	4.4	1.1	1.4	0.5	0.3	Bal.
C-4	1.4	5.2	4.5	1.0	1.3	0.5	0.3	Bal.

Table 1 compositions of the coatings

3. Micro-structure of coatings

3.1. XRD results of coatings

The XRD result is shown in Fig. 1. The coatings are mainly com-posed of NbC, a phase (martensite) and c phase (retained austenite). The variation of tetragonality in the martensite crystals can be revealed by the X-ray peak profiles. It is noted that the a phase came out peaks shift caused by lattice constant changes and dis-solved C contents [32]. And the peaks of a phase show considerable broadening, which indicates the grain refinement of the marten-site. Furthermore, the retained austenite appears in C-3 and C-4 coatings. Besides, the peaks shift of NbC can also be seen and none of other peak could be observed in any coating.

3.2. Micro-structure of coatings

The micro-structures of coatings are shown in Fig. 2. Apparent morphologies variation of NbC could be seen in coatings. Reticular NbC and small rod NbC could be observed in C-1 coating, which are replaced by granular NbC and small rod NbC in C-2, C-3 and C-4 coatings. With the increase of C content, a reduction of the amount of small rod NbC could be seen. Moreover, the size and amount increasing of granular NbC could also be found. Notably, some flaky structures and cracks can be seen only in C-4 coating.

4. Hardness and wear resistance of coatings

Since the matrix of coatings have been affected significantly by C contents from the result of XRD, it is necessary to measure the hardness of matrix. The average Vickers hardness of matrix (the area without NbC) and Rockwell hardness of coatings with different C contents are shown in Fig. 3. A significant increase of the hardness of matrix can be seen and the hardness of C-4 coating (780 HV) is slightly higher than that of C-3 coating (750 HV), which is much higher than those of C-1 coating (270 HV) and C-2 coating (550 HV). The Rockwell hardness of coatings perform a similar result. The hardness of C-4 coating is the highest (HRC 59) and the hardness of C-3 coating is slightly lower (HRC 58) than that of C-4 coating. The hardness of C-1 and C-2 coatings are HRC 22 and HRC 48 respectively.

The wear loss of the coatings with different C contents are shown in Fig. 4. It could be found that the wear resistance of each coating performs significant alterations with different C contents. The wear loss of C-3 coating is 0.27 g/N cm2 in 8 h, which is the lowest in all coatings. The wear loss of C-4 coating is slightly higher than that of C-3 coating, which is inconsistent with the hardness tendency. To achieve a better understand of wear resistance, the worn surfaces morphologies of the C-3 and C-4 coatings are illustrated in Fig. 5. Both of C-3 and C-4 coatings present numerous similar furrows paralleling to each other on the surface, and C-4 coating is slightly smoother than C-3 coating, which benefit from the slightly higher hardness of matrix. It is noteworthy that, some broken area could be observed in C-4 coating and one of them is shown in Fig. 5(b). Discussion

As shown in Fig. 4, the wear resistance of coatings presents a decrease when C contents increase to 1.4 wt.%. The main factors impacting wear resistance of these coatings are the hardness of matrix, the morphology of NbC, the hardness of NbC and the defects of coatings. The hardness variations of coatings and matrix have been investigated before. Therefore, the morphology changes of NbC the hardness of NbC and the source of defects will be discussed as follows.

5.1. Morphology of NbC

In this work, the morphologies of NbC include granular NbC, small rod NbC and reticular NbC. Morphology changes of NbC mainly depend on the formation sequence of NbC and matrix. The equilibrium phase diagram of the coating is shown in Fig. 6. The phase diagram contains liquid phase, NbC, γ phase, α phase, M_7C_3 and $M_{23}C_6$. The granular NbC precipitates out earlier than matrix. The small rod NbC precipitates out together with matrix. And the reticular NbC precipitates out at grain boundary just after solidification of matrix. It could be observed that the solidification mode of C-1 coating is $L \rightarrow L + \alpha \rightarrow L + \alpha + NbC \rightarrow \alpha + NbC$. The precipitation temperature of NbC is 1432 ℃, which is lower than that of α phase (1437 ℃) and both of them are finished at a slightly lower temperature 1419 ℃. It is learned that the granular NbC can-not form in C-1 coating, replaced by small rod NbC and reticular NbC, which has been mentioned in Fig. 2(a). The solidification modes of C-2, C-3 and C-4 coatings are $L \rightarrow L + NbC \rightarrow L + \gamma + NbC \rightarrow \gamma + NbC$. The precipitation temperatures of NbC are 1527 ℃, 1597 ℃ and 1627 ℃ respectively, which are earlier than those of γ phase (1429 ℃, 1420 LC and 1413 ℃). Granular NbC can separate out from liquid phase. Furthermore, the precipitation temperature interval between NbC and γ phase is broadened with the increase of C content, which can cause the slightly size increase of granular NbC and the obviously amount decrease of small rod NbC.

5.2. Theoretical hardness of NbC and carbon poor niobium carbides in coatings

The hardness of NbC, which has an important effect on wear resistance should be learned. However, it is difficult to get the hardness value of NbC by experiment in this work due to their sizes and crystal orientations, which could have a huge impact on hardness [33]. Therefore, the theoretical hardness calculation of NbC and carbon-poor niobium carbide is needed to give a trend of hardness changes caused by carbon vacancy.

The NbC and carbon poor niobium carbide models are shown in Fig. 7. The formation energy increase and lattice parameter decrease of the NbC_x have been reported [24,34]. The Bulk modulus (B) and Shear modulus (G) can be obtained directly from calculations. The elastic modulus (E) and Poisson's ratio (m) could be obtained from B and G by the following relationship:

$$E = 9BG / (3B + G) \tag{1}$$

$$v = (3B - 2G) / 2(3B + G) \tag{2}$$

All these calculated results together with the previously published results are listed in Table.2. The theoretical hardness can be get by Eq. (3) [35]:

$$H_{cal} = 0.92K^{1.137}G^{0.708}, K = G/B \tag{3}$$

The calculated hardness of NbC, $NbC_{0.75}$ and $NbC_{0.5}$ are shown in Fig. 8. The hardness value of NbC in this work is 24.5 GPa, which coincides well with other previously published results [36]. The hardness of $NbC_{0.75}$ and $NbC_{0.5}$ are 13.8 GPa and 6.5 GPa, respectively. It can be seen clearly that lack of carbon can dramatically decrease the hardness of niobium carbides. The brittleness of these carbides can be assessed by the Pugh's modulus ratio 'K', and the carbide equipped with brittle character when 'K' is bigger than 0.571. From Fig. 8(b), the values of $NbC_{0.75}$ and $NbC_{0.5}$ are smaller than 0.571, which indicate that lack of carbon can decrease the brittleness of niobium carbides.

The calculation results show that lattice parameter of niobium carbides is decreased with the decrease of C content. From the XRD results (Fig. 1), the peaks shift of niobium carbides can be seen and it is believed that this change was caused by C contents variation in niobium carbides. So, it is reasonable to make a comparison of lattice parameter between theoretical calculation and XRD results to estimate the hardness and brittleness of niobium carbides in different coatings. Lattice parameter of NbC and $NbC_{0.75}$ are 4.469 Å and 4.427 Å. According to the well known Bragg's law, the 2θ ((1 1 1) crystal plane) value of the two carbides are 34.739° and 35.077°. The 2θ ((1 1 1) crystal plane) value of car-bides in four coatings are 34.90° (C-1), 34.80° (C-2) and 34.78° (C-3, C-4). As shown in Fig. 9, the estimated hardness of carbides in four coatings are 19.4 GPa(C-1), 22.5 GPa(C-2) and 23.2 GPa(C-3, C-4). The G/B value of carbides are 0.573(C-1), 0.622(C-2) and 0.631 GPa(C-3, C-4). The hardness and brittleness of niobium carbides in coatings are increased obviously with the increase of C content. Considering the lattice misfit (d) between ferrite and carbide, a contraction of NbC_x is of great significance. The crystallographic orientation of the ferrite with the NaCl type carbide usually has a Baker-Nutting relationship [37]: $(100)_a \| (100)_{NbC_x} [010]_a \| [011]_{NbC_x}$, and the lattice misfit can be obtained by Eq. (4):

$$\delta = (a_{carbide} - \sqrt{2}a_a) / a_{carbide} \tag{4}$$

The calculated lattice parameters of a_{NbC}, $a_{NbC_{0.75}}$ and a_a are 4.469 Å, 4.427 Å and 2.873 Å, respectively. The misfit of NbC with ferrite is 8.7% and it decreases to 8.2% in the case of $NbC_{0.75}$ which is beneficial to the coherency of carbides with Fe matrix.

5.3. Flaky structure and cracks on C-4 coating

The flaky structure has been found in C-4 coating, which is shown in Fig. 10(a) and its composition is listed in Table.3. By using energy spectroscopy, the structures, which are mainly composed of elements Fe, Cr, C, can be alternatively supposed to be M_7C_3 or $M_{23}C_6$, according to the equilibrium phase diagram. $M_{23}C_6$ is usu-ally obtained by the diffusion controlled transformation $M_7C_3 \rightarrow M_{23}C_6$ [38] during cooling, and the transformation does not occur in high cooling rate [39–42]. Furthermore, the formation of $M_{23}C_6$ is in connection with Cr percentage with a lower limit of around 60 wt.% [39]. Considering the high cooling rate of welding process and Fe, Cr, C percentage of the structure, the flaky structure is supposed to be M_7C_3. It is noteworthy that part desquamation of M_7C_3 can be seen in Fig. 10(a) and the hole like structure remains after M_7C_3 carbide entire desquamation which is shown in Fig. 10(b). Some cracks can be seen growing on the edge of M_7C_3.

5.4. Wear resistance of coatings

The wear resistance of the coatings is shown in Fig. 5, in which, that of C-4 coating is decreased compared with that of C-3 one. Obvious variation of coatings could be seen with the increase of C contents. The increase of hardness of coatings, matrix and niobium carbides would increase the wear resistance of C-4 coating. And the morphology changes of NbC may also indicate that the increase of the wear resistance of C-4 coating is related with granular NbC, which is supposed to be the best morphology [43,44]. However, the hole like structures (Fig. 10(b)) which resulting from the desquamation of flaky

M_7C_3 turn into broken area (Fig. 5(b)) during wear process. The desquamation of flaky and the M_7C_3 cracks nearby may be the major factor to decrease the wear resistance of C-4 coating.

5. Acknowledgement

6.Conclusions

(1) Distribution and morphology of NbC are changed obviously and they tend to separate out in form of granular with the increase of C content.

(2) Lack of carbon can decrease the hardness and brittleness of NbCx carbides and decrease the misfit of niobium carbides with the Fe matrix.

(3) The flaky M_7C_3 separate out at 1.4 wt.% C and the desquamation of the carbides decrease the wear resistance of coating.

(4) The coating with 1.2 wt.%C content is equipped with the best wear resistance.

References

[1] A. Emamian, S.F. Corbin, A. Khajepour, Effect of laser cladding process parameters on clad quality and in-situ formed microstructure of Fe–TiC composite coatings, Surf. Coat. Technol. 205 (2010) 2007–2015.

[2] D. Ravnikar, N.B. Dahotre, J. Grum, Laser coating of aluminum alloy EN AW 6082-T651 with TiB2 and TiC: microstructure and mechanical properties, Appl. Surf. Sci. 282 (2013) 914–922.

[3] K. Liu, Y. Li, J. Wang, Q. Ma, Effect of high dilution on the in situ synthesis of Ni– Zr/Zr–Si(B, C) reinforced composite coating on zirconium alloy substrate by laser cladding, Mater. Des. 87 (2015) 66–74.

[4] Z.-H. Zhang, X.-B. Shen, S. Wen, J. Luo, S.-K. Lee, F.-C. Wang, In situ reaction synthesis of Ti–TiB composites containing high volume fraction of TiB by spark plasma sintering process, J. Alloys Compd. 503 (2010) 145–150.

[5] K.L. Wang, Q.B. Zhang, M.L. Sun, X.G. Wei, Microstructural characteristics of laser clad coatings with rare earth metal elements, J. Mater. Process. Technol. 139 (2003) 448–452.

[6] Q. Li, Y. Lei, H. Fu, Growth characteristics and reinforcing behavior of in-situ NbCp in laser cladded Fe-based composite coating, J. Mater. Sci. Technol. 31 (2015) 766–772.

[7] Q. Li, Y. Lei, H. Fu, Laser cladding in-situ NbC particle reinforced Fe-based composite coatings with rare earth oxide addition, Surf. Coat. Technol. 239 (2014) 102–107.

[8] S. Barzilai, A. Raveh, N. Frage, Inter-diffusion of carbon into niobium coatings deposited on graphite, Thin Solid Films 496 (2006) 450–456.

[9] S.G. Huang, R.L. Liu, L. Li, O.V.D. Biest, J. Vleugels, NbC as grain growth inhibitor and carbide in WC–Co hardmetals, Int. J. Refract Metal Hard Mater. 26 (2008) 389–395.

[10] R. Colaço, R. Vilar, Laser rapid-alloy prototyping for the development of wear resistant Fe–Cr–C/NbC composite materials, J. Laser Appl. 15 (2003) 267–272.

[11] X. Niu, M.J. Chao, W.L. Wang, B. Yuan, E.J. Liang, In situ synthesized NbC particulate reinforced Ni-based composite coatings by laser cladding, Chin. J. Lasers 33 (2006) 987–992.

[12] C. Wu, M. Ma, W. Liu, M. Zhong, W. Zhang, H. Zhang, Laser producing Fe-based composite coatings reinforced by in situ synthesized multiple carbide particles, Mater. Lett. 62 (2008) 3077–3080.

[13] N. Zhao, Y. Xu, Y. Fu, Mechanical properties of one-step in situ synthesized NbC-Fe composite coating, Surf. Coat. Technol. 309 (2017) 1105–1110.

[14] R.A. Mesquita, C.A. Schuh, Tool steel coatings based on niobium carbide and carbonitride compounds, Surf. Coat. Technol. 207 (2012) 472–479.

[15] Y. Higashigawa, T. Kohara, M. Morita, M. Akiyama, Estimation of roles of matrix and NbC particles dispersed in surface layer of tool by PTA welding, Procedia Eng. 81 (2014) 1927–1932.

[16] S. Qin, B. Liao, L. Mao, F. Xiao, A novel method for preparing nano-NbC/Fe powder and nano-NbC particle reinforced cast low-carbon steel, Mater. Lett. 121 (2014) 162–165.

[17] X.H. Wang, Z.D. Zou, S.Y. Qu, S.L. Song, Microstructure and wear properties of Fe-based hardfacing coating reinforced by TiC particles, J. Mater. Process. Technol. 168 (2005) 89–94.

[18] H.R. Jafarian, E. Borhani, A. Shibata, D. Terada, N. Tsuji, Martensite/austenite interfaces in ultrafine grained Fe–Ni–C alloy, J. Mater. Sci. 46 (2011) 4216– 4220.

[19] T. Maki, K. Tsuzaki, I. Tamura, The morphology of microstructure composed of lath martensite in steels, Adv. Astr. Square Kilometre Array 20 (1980) 207– 214

[20] G. Krauss, A.R. Marder, The morphology of martensite in iron alloys, Metall. Trans. 2 (1971) 2343–2357.

[21] G. Krauss, Martensite in steel: strength and structure, Mater. Sci. Eng. A s 273– 275 (1999) 40–57.

[22] M. Umemoto, E. Yoshitake, I. Tamura, The morphology of martensite in Fe-C, Fe-Ni-C and Fe-Cr-C alloys, J. Mater. Sci. 18 (1983) 2893–2904.

[23] G. Miyamoto, N. Iwata, N. Takayama, T. Furuhara, Mapping the parent austenite orientation reconstructed from the orientation of martensite by EBSD and its application to ausformed martensite, Acta Mater. 58 (2010) 6393–6403.

[24] J.H. Jang, C.-H. Lee, Y.-U. Heo, D.-W. Suh, Stability of (Ti, M)C (M = Nb, V, Mo and W) carbide in steels using first-principles calculations, Acta Mater. 60 (2012) 208–217.

[25] J. Xu, J. Cheng, S. Jiang, P. Munroe, Z.-H. Xie, The influence of Ti additions on the mechanical and electrochemical behavior of b-Ta_5Si_3 nanocrystalline coating, Appl. Surf. Sci. 419 (2017) 901–915.

[26] P. Zhang, Y. Zhou, J. Yang, D. Li, X. Ren, Y. Yang, Q. Yang, Optimization on mechanical properties of Fe7 xCrxC3 carbides by first-principles investigation, J. Alloys Compd. 560 (2013) 49–53.

[27] N.R. Mediukh, P.E.A. Turchi, V.I. Ivashchenko, V.I. Shevchenko, First-principles calculations for the mechanical properties of Ti-Nb-B2 solid solutions, Comput. Mater. Sci. 129 (2017) 82–88.

[28] X. Yun, Y.F. Zhou, B. Zhao, X.L. Xing, J. Yang, Y.L. Yang, Q.X. Yang, Influence of nano-Y2O3 on wear resistance of hypereutectic Fe–Cr–C hardfacing coating, Tribol. Lett. 58 (2015).

[29] D. Vanderbilt, Soft self-consistent pseudopotentials in a generalized eigenvalue formalism, Phys. Rev. B 41 (1990) 7892–7895.

[30] J.P. Perdew, E.R. McMullen, A. Zunger, Density-functional theory of the correlation energy in atoms and ions: a simple analytic model and a challenge, Phys. Rev. A 23 (1981) 2785–2789.

[31] W. Boas, Physical properties of crystals, their representation by tensors and matrices: J.F Nye: Clarendon Press, Oxford, 1957. 322pp., 50s, J. Mech. Phys. Solids 6 (1958) 328–329.

[32] B. Hutchinson, J. Hagström, O. Karlsson, D. Lindell, M. Tornberg, F. Lindberg, M. Thuvander, Microstructures and hardness of as-quenched martensites (0.1– 0.5%C), Acta Mater. 59 (2011) 5845–5858.

[33] Y. Kumashiro, A. Itoh, T. Kinoshita, M. Sobajima, The micro-Vickers hardness of TiC single crystals up to 1500L C, J. Mater. Sci. 12 (1977) 595–601.

[34] A. Teresiak, H. Kubsch, X-ray investigations of high energy ball milled transition metal carbides, Nanostruct. Mater. 6 (1995) 671–674.

[35] Y. Tian, B. Xu, Z. Zhao, Microscopic theory of hardness and design of novel superhard crystals, Int. J. Refract Metal Hard Mater. 33 (2012) 93–106.

[36] L. Wu, Y. Wang, Z. Yan, J. Zhang, F. Xiao, B. Liao, The phase stability and mechanical properties of Nb–C system: using first-principles calculations and nano-indentation, J. Alloys Compd. 561 (2013) 220–227.

[37] A.M. Nartowski, I.P. Parkin, M. Mackenzie, A.J. Craven, Solid state metathesis: synthesis of metal carbides from metal oxides, J. Mater. Chem. 11 (2001) 3116–3119.

[38] M. Kowalski, P.J. Spencer, K. Granat, H. Drzeniek, E. Lugscheider, Phase relations in the C-Cr-Fe system in the vicinity of the /liquid + bcc + M23C6 + M7C3/invariant equilibrium – experimental determinations and thermodynamic modelling, 1994.

[39] A. Wiengmoon, Carbides in High Chromium Cast Irons, 2011.

[40] J.T.H. Pearce, D.W.L. Elwell, Duplex nature of eutectic carbides in heat treated 30% chromium cast iron, J. Mater. Sci. Lett. 5 (1986) 1063–1064.

[41] A. Wiengmoon, T. Chairuangsri, A. Brown, R. Brydson, D.V. Edmonds, J.T.H. Pearce, Microstructural and crystallographical study of carbides in 30 wt.%Cr cast irons, Acta Mater. 53 (2005) 4143–4154.

[42] K. Wieczerzak, P. Bala, R. Dziurka, T. Tokarski, G. Cios, T. Koziel, L. Gondek, The effect of temperature on the evolution of eutectic carbides and M7C3 ? M23C6 carbides reaction in the rapidly solidified Fe-Cr-C alloy, J. Alloys Compd. 698 (2017) 673–684.

[43] J.W. Park, C.L. Huo, S. Lee, Composition, microstructure, hardness, and wear properties of high-speed steel rolls, Metall. Mater. Trans. A 30 (1999) 399–409.

[44] S. Wei, J. Zhu, L. Xu, R. Long, Effects of carbon on microstructures and properties of high vanadium high-speed steel, Mater. Des. 27 (2006) 58–63.

Phase	Lattice constants	Elastic modulus	Bulk modulus	Shear modulus	Passion ratio	Formation energy
	a (Å)	E (GPa)	B (GPa)	G (GPa)	m	E_{for} (eV/atom)
NbC	4.469	509	316	206	0.23	0.63
	4.468 [34], 4.47 [37]	486 [36]	318 [24]		0.22 [36]	0.56 [36], 0.73 [24]
$NbC_{0.75}$	4.427	355	282	138	0.29	0.47
$NbC_{0.5}$	4.341, 4.467(c)	229	248	85	0.34	0.35

Table 2 Calculated results of lattice constant, Elastic modulus, Bulik modulus, Shear modulus, passion ratio and formation energy.

Chemical element	Weight percentage	Atom percentage
Si	0.5	0.68
V	3.42	2.55
Cr	30.62	22.38
Mn	1.89	1.31
Fe	51.54	31.06
C	12.02	38.02

Table 3 EDS analysis results of Area 1.
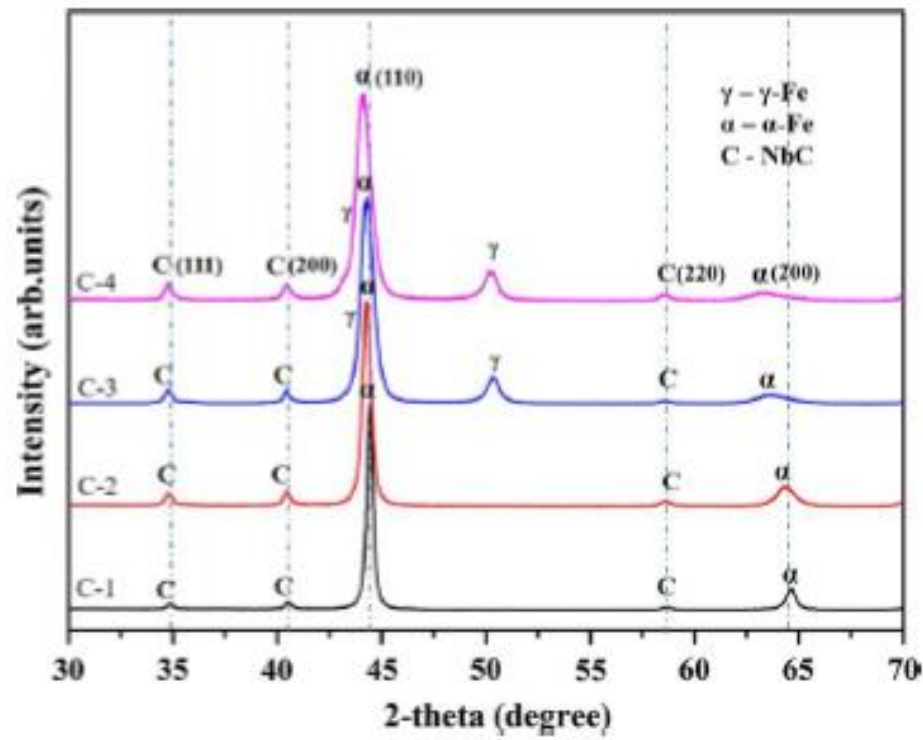
Fig. 1. XRD results of coatings.
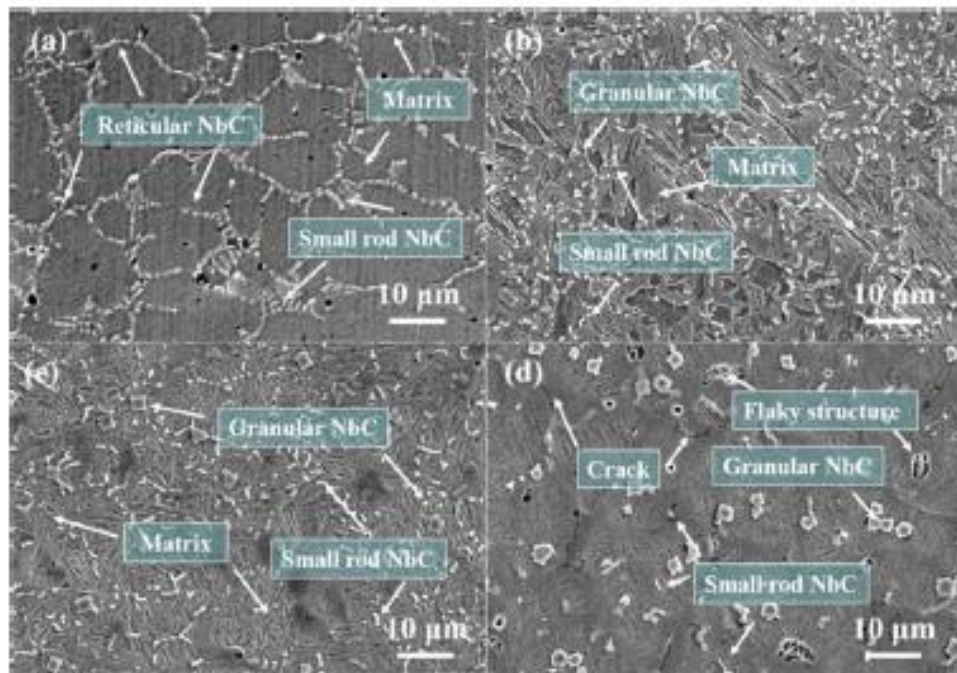
Fig. 2. Micro-structure of coatings (a) C-1, (b) C-2, (c) C-3, (d) C-4.
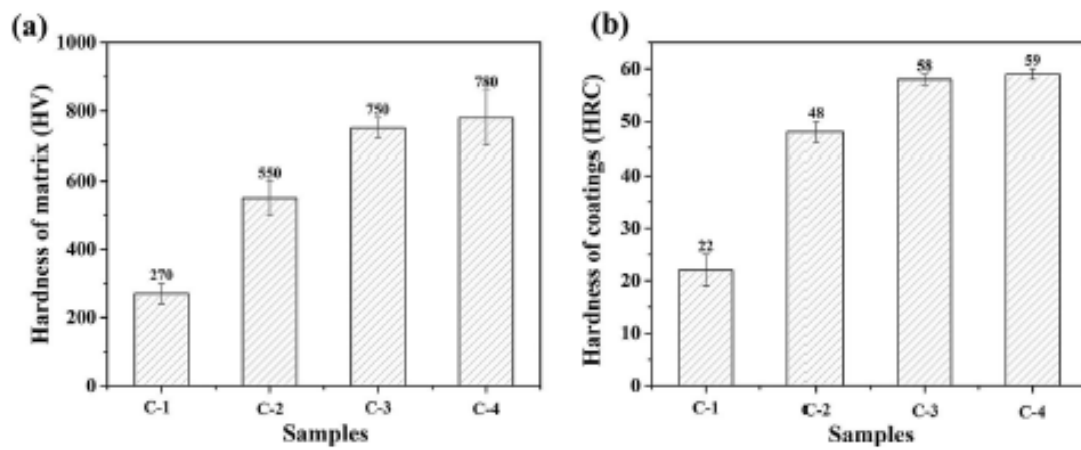
Fig. 3. Hardness of matrix and coatings (a) matrix, (b) coatings.
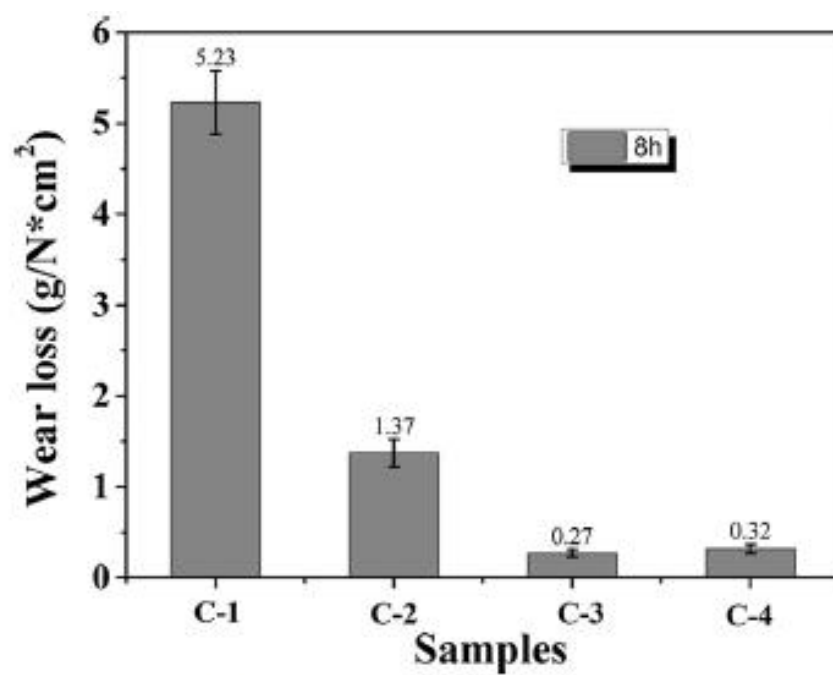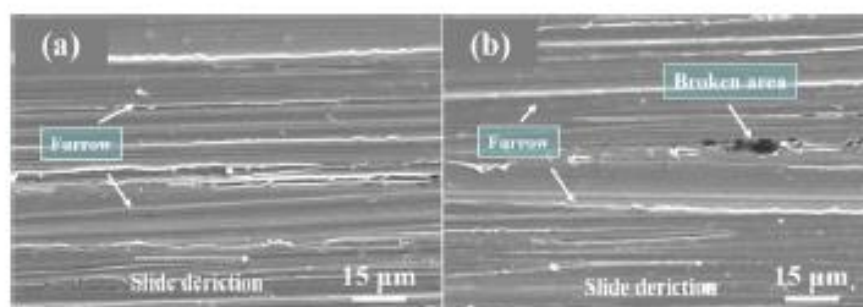
.Fig. 4. Wear resistance analysis of coatings

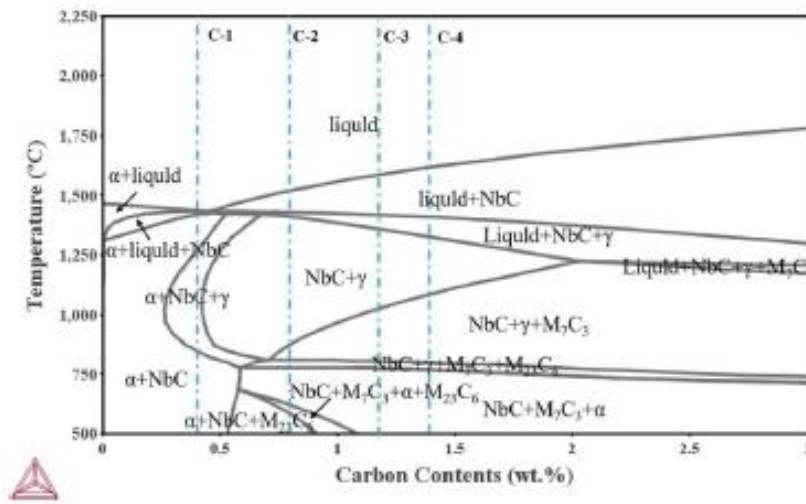Fig. 5. Wear surfaces morphology of the coatings (a) C-3, (b) C-
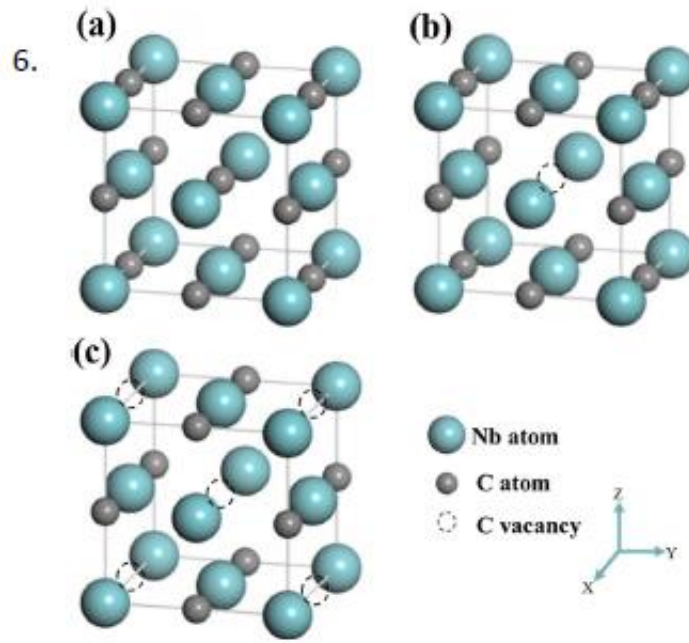
Fig. 6. Equilibrium phase diagram of coatings.

6.

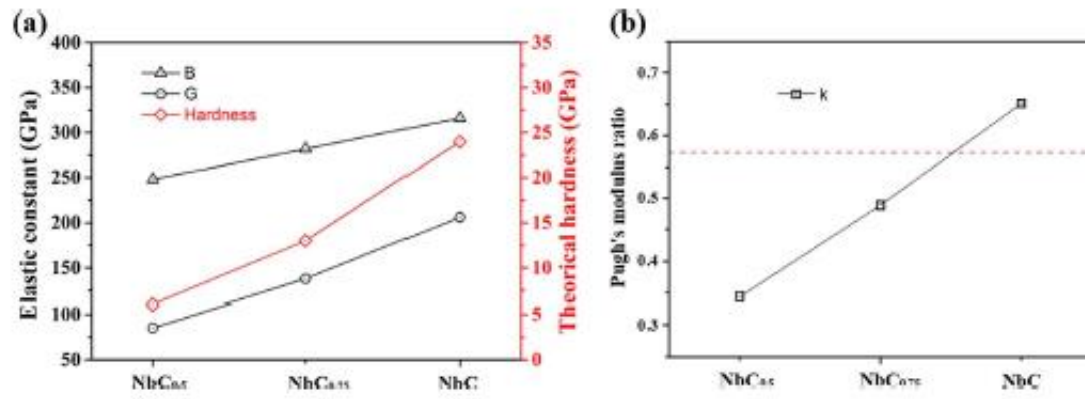Fig. 7. Calculation models of niobium carbides (a) NbC, (b) NbC0.75, (c) NbC0.5.

Fig. 8. Theoretical hardness and brittleness of niobium carbides
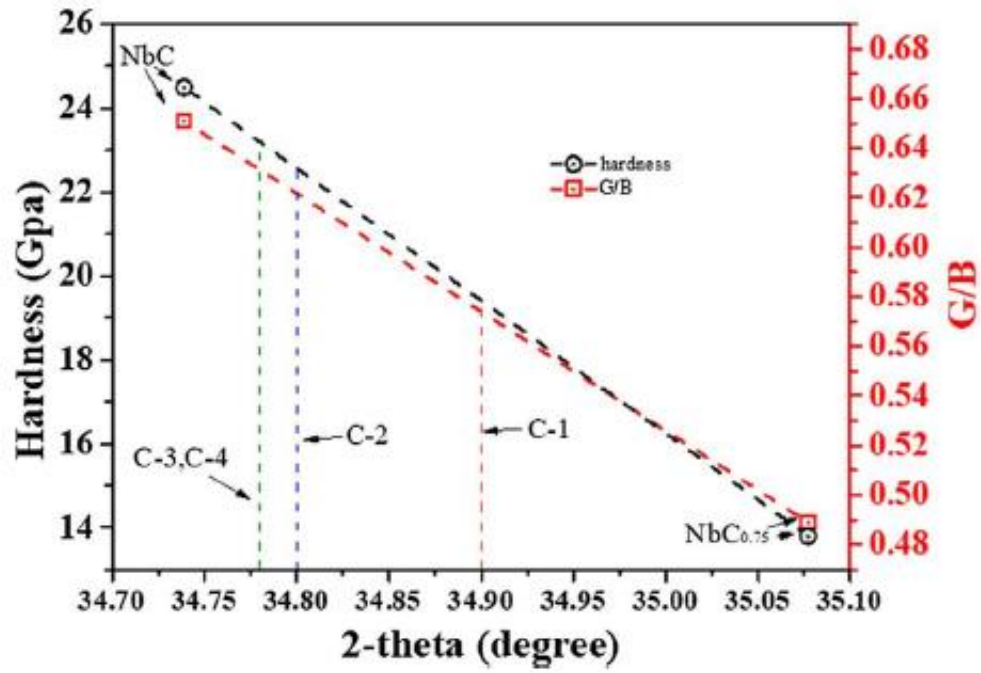(a) Theoretical hardness. (b) Pugh's modulus ratio.

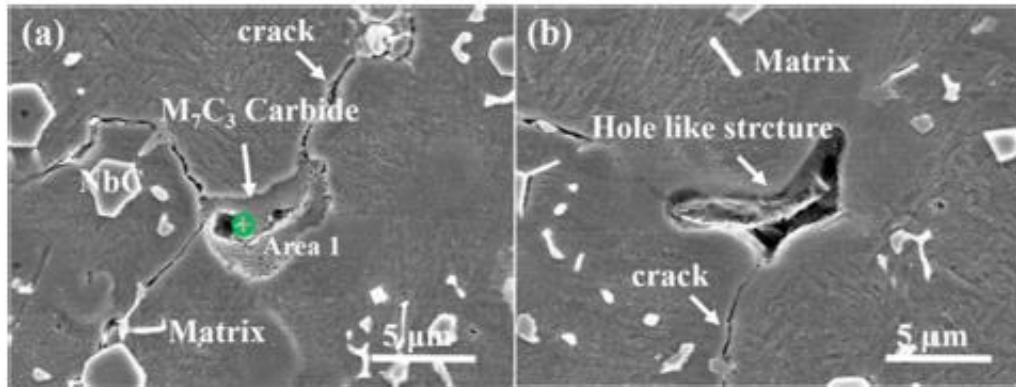Fig. 9. Hardness and brittleness estimation of niobium carbides in four coatings.

Fig. 10. Morphology of flaky structures in C-4 coating (a) Morphology of M_7C_3 of before entire desquamation. (b) Morphology of M_7C_3 after entire desquamation.